Description of nuclear octupole and quadrupole deformation close to axial symmetry: Critical-point behavior of ^{224}Ra and ^{224}Th

P. G. Bizzeti* and A. M. Bizzeti-Sona

Dipartimento di Fisica, Universitá di Firenze, I.N.F.N., Sezione di Firenze, Via G. Sansone 1, I-50019 Sesto Fiorentino (Firenze), Italy

(Received 13 December 2007; published 29 February 2008)

The model, introduced in a previous paper, for the description of the octupole and quadrupole degrees of freedom in conditions close to axial symmetry, is applied to situations of shape phase transitions where the quadrupole amplitude can reach zero. The transitional nuclei ^{224,226}Ra and ^{224}Th are discussed in the frame of this model. Their level schemes can be reasonably accounted for by assuming a square-well potential in two dimensions. Electromagnetic transition amplitudes are also evaluated and compared with existing experimental data.

DOI: 10.1103/PhysRevC.77.024320 PACS number(s): 21.60.Ev, 21.10.Re, 21.10.Ft, 27.90.+b

I. INTRODUCTION

The phase transition between spherical and axially deformed quadrupole shapes of nuclei has been the object of several theoretical and experimental works in recent years. In particular, the properties of nuclei close to the critical point, predicted by Iachello's model of X(5) symmetry [1], have been actually observed in several cases [2–7], and some other nuclides showing the ratio $E(4^+)/E(2^+) \approx 2.91$ expected for X(5) symmetry are presently under investigation. Moreover, in the Ra-Th region, it has been observed that the isotopes ^{224}Ra and ^{224}Th have a positive-parity ground-state band with a sequence of level energies very close to the X(5) predictions [8,9]. Here, however, the presence of a very low lying negative-parity band, soon merging with the positive-parity one for $J > 5$, proves that the octupole mode of deformation plays an important role and should not be ignored in discussing the behavior of the phase transition.

In a previous paper [10] (henceforth referred to as I) a simple model has been introduced to describe the phase transitions in nuclear shape involving the octupole mode.[1] To this purpose, a new parametrization of the collective coordinates describing the nuclear quadrupole and octupole deformation has been introduced and discussed. The nuclear shape is represented in the intrinsic frame defined by the principal axes of the overall tensor of inertia, in situations close to (but not necessarily coincident with) the axial-symmetry limit. In the same paper, a specific model is developed to describe the critical point of the phase transition in the octupole mode, between harmonic oscillations and permanent asymmetric deformation, in nuclei that already possess a stable quadrupole deformation. The thorium isotopic chain was investigated and the experimental data concerning ^{226,228}Th were compared with the model predictions [10]. The former appears to be close to the critical point, whereas the latter can be interpreted as an example of harmonic oscillations in the axial octupole mode.

In the present paper, we extend the investigation to the cases where the quadrupole deformation is not steady but performs oscillations under the effect of a proper potential, and in particular for situations close to the quadrupole critical point described by X(5) symmetry, in the radium and thorium isotopic chain.

As we shall see, the properties of the already mentioned nuclei ^{224}Th and ^{224}Ra are reasonably described by our model with a "critical" (flat) potential well, extending both in the β_2 and β_3 directions. Moreover, we observe that, as far as the level scheme is concerned, the next isotope ^{226}Ra can also be accounted for with a proper critical-point potential, in spite of the fact that the positive-parity part of the ground-state band does not follow the X(5) predictions. As in the case of thorium, heavier isotopes of radium have a permanent quadrupole deformation and octupole excitations of vibrational character, whereas the lighter ones are either noncollective or vibrational in the quadrupole mode.

Some results of this work, at different phases of advancement, have been reported at several conferences or schools [9,11–13].

For convenience of the reader, we report in the next section some evidence of the phase transitions in the radium and thorium isotopic chain, and the definition of variables introduced in I and a few results relevant to the present work are briefly summarized in Sec. III A. In the remainder of Sec. III, the model introduced in I is specialized to a form suitable for a critical potential in two dimensions. Finally, in Sec. IV the model results are reported and compared with the existing experimental evidence for ^{224,226}Ra and ^{224}Th. Previous models of quadrupole-octupole deformation are quoted in I. Since then, new relevant papers have appeared. A new analytic quadrupole-octupole axially symmetric model (AQOA) has been proposed by Bonatsos *et al.* [14] to discuss the evolution of the quadrupole and octupole collectivity in Ra and Th isotopes. A parameter-free model starting from a similar approach has been developed by Lenis and Bonatsos [15] and compared with the experimental results for ^{226}Ra and ^{226}Th. Moreover, a variant of the AQOA model, introducing a renormalization of the nuclear moment of inertia [16], has

*bizzeti@fi.infn.it

[1] We have now the occasion to correct a few misprints that escaped proofreading in paper I: Equation (23c) should read $q_3 = (L_3 - p_\varphi - 2p_\chi - 3p_\vartheta)/(4u_0^2)$. In Table VII, the fourth element of the fifth line should be $\sin\theta_2 \sin\theta_3/\mathcal{J}_1$. We apologize for these errors.

been used to describe the lowest quadrupole and octupole bands of the $N = 90$ isotones ^{150}Nd, ^{152}Sm, ^{154}Gd, and ^{156}Dy. A discussion of the octupole bands of ^{150}Nd and ^{152}Sm can be found in Refs. [9,12]. Finally, an extension of the extended coherent state model [17] has been developed by Raduta and co-workers [18–20], which also includes the lowest $K^\pi = 1^+$ and 1^- bands in the model space, and the model predictions have been compared with the experimental data for several nuclei of the regions of the actinides and of the rare earths.

II. PHASE TRANSITIONS IN THE RA-TH REGION

We summarize here the existing evidence for the evolution of nuclear shapes for radium and thorium isotopes in the transitional region $N = 130$–140.

Figure 1, taken from I, shows the behavior of some indicators of quadrupole and octupole collectivity, as a function of the neutron number N, in the isotopic chain of Ra and Th. It has been noted in I that ^{226}Th appears to be close to the critical point in the octupole deformation, but it possesses a stable quadrupole deformation β_2. At larger values of N, Th isotopes maintain a stable quadrupole deformation, whereas the octupole mode evolves toward the vibrational behavior, as indicated by the large excitation energies of all negative-parity levels. At $N = 130$ or less, the quadrupole mode has a vibrational (or noncollective) character. It turns out, therefore, that the octupole phase transition proceeds in the direction opposite to the quadrupole one. We also observe that the phase transition only involves the axial octupole mode. In fact, the energy of the $J^\pi = 1^-$ bandhead of the $K^\pi = 0^-$ octupole band shows a sharp decrease, both in its absolute value and in the ratio to $E(2^+)$, when the neutron number decreases below $N = 142$. Other octupole bands (with $K > 0$) do not show a similar trend [Fig. 1(c)], and one can conclude that nonaxial octupole excitations maintain a vibrational character. A similar trend is apparent also for Ra isotopes.

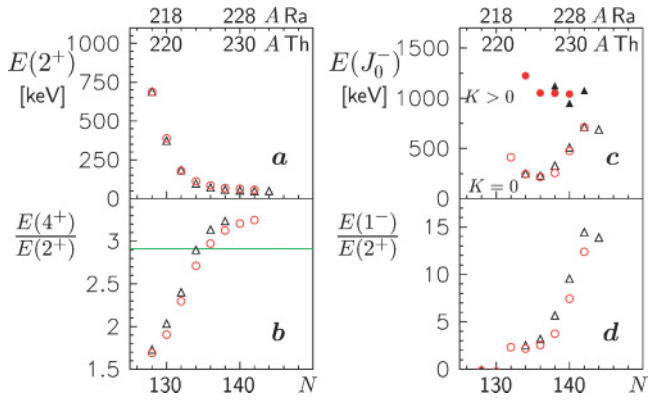

FIG. 1. (Color online) Indicators of the quadrupole collectivity (left) and of the octupole collectivity (right), as a function of the neutron number N in the isotopic chain of Ra (circles) and Th (triangles). (a) Excitation energy of the first 2^+ level. (b) Energy ratio $E(4^+)/E(2^+)$. (c) Excitation energy of the first level of the $K^\pi = 0^-$ band, $J_0^\pi = 1^-$ (open symbols), and of the lowest known level of other negative-parity bands, $J_0^\pi = 2^-$ or 1_2^- (full symbols). (d) Energy ratio $E(1^-)/E(2^+)$. The horizontal line in (b) shows the value (2.91) expected for the X(5) symmetry (from Ref. [10]).

To describe Th and Ra isotopes with $A < 226$, we must also allow β_2 to vary and perform (not necessarily harmonic) oscillations. If we consider the value $E(4^+)/E(2^+) = 2.91$ as a signature of the critical point with respect to the quadrupole deformation, this would correspond approximately to ^{224}Ra and ^{224}Th.

III. THE MODEL FOR QUADRUPOLE-OCTUPOLE VIBRATIONS

A. Summary of the variable definitions

The dynamical variables $a_\mu^{(\lambda)}$ ($\lambda = 2, 3; \mu = -\lambda, \ldots, \lambda$), describing the quadrupole and octupole deformation in the intrinsic reference frame, are parametrized as

$$\begin{aligned}
a_0^{(2)} &= \beta_2 \cos\gamma_2 \approx \beta_2, \\
a_1^{(2)} &= -\frac{\sqrt{2}\beta_3}{\sqrt{\beta_2^2 + 2\beta_3^2}} v(\sin\varphi + i\cos\varphi), \\
a_2^{(2)} &= \sqrt{1/2}\beta_2 \sin\gamma_2 - i\frac{\sqrt{5}\beta_3}{\sqrt{\beta_2^2 + 2\beta_3^2}} u \sin\chi, \\
a_0^{(3)} &= \beta_3 \cos\gamma_3 \approx \beta_3, \\
a_1^{(3)} &= \frac{\sqrt{5}\beta_2}{\sqrt{\beta_2^2 + 2\beta_3^2}} v(\sin\varphi + i\sin\varphi), \\
a_2^{(3)} &= \sqrt{1/2}\beta_3 \sin\gamma_3 + i\frac{\beta_2}{\sqrt{\beta_2^2 + 2\beta_3^2}} u \sin\chi, \\
a_3^{(3)} &= w\sin\vartheta\left[\cos\gamma_3 + (\sqrt{15}/2)\sin\gamma_3\right] \\
&\quad + iw\cos\vartheta\left[\cos\gamma_3 - (\sqrt{15}/2)\sin\gamma_3\right] \\
&\approx w(\sin\vartheta + i\cos\vartheta).
\end{aligned} \tag{1}$$

With this choice, valid in situations close to axial symmetry, the tensor of inertia turns out to be diagonal *up to first order* in the *small* quantities describing the nonaxial deformations.

In Eqs. (1) the variables γ_2 and γ_3 are still employed, to keep some transparency with respect to the standard expressions used to describe the quadrupole [21] or the octupole deformation alone [22]. However, it is more convenient to substitute them with expressions involving the variables u, χ and a new variable u_0: Neglecting second-order and higher-order terms gives

$$\begin{aligned}
\gamma_2 &= \frac{\sqrt{10}\beta_3}{\beta_2\sqrt{\beta_2^2 + 5\beta_3^2}} u\cos\chi + \frac{f(\beta_2,\beta_3)}{\sqrt{\beta_2^2 + 5\beta_3^2}} u_0, \\
\gamma_3 &= -\frac{\sqrt{2}\beta_2}{\beta_3\sqrt{\beta_2^2 + 5\beta_3^2}} u\cos\chi + \frac{\sqrt{5}f(\beta_2,\beta_3)}{\sqrt{\beta_2^2 + 5\beta_3^2}} u_0.
\end{aligned} \tag{2}$$

It is possible to show that a definite value of the angular-momentum component K along the intrinsic axis 3 and a definite parity can be associated with the degrees of freedom corresponding to the variables v, χ (or u, φ or w, ϑ or u_0): $K^\pi = 1^-$ (or 2^- or 3^- or 2^+, respectively). This result is independent of the form of the function $f(\beta_2, \beta_3)$ of Eq. (2) (which, actually, was left undetermined in I).

TABLE I. The matrix of inertia $\mathcal{G}$ after the introduction of the variables $u_0, v, u, w, \varphi, \chi$, and ϑ (see text). Here, $\mathcal{J}_1 = \mathcal{J}_2 = 3(\beta_2^2 + 2\beta_3^2)$ and $\mathcal{J}_3 = 4f^2(\beta_2, \beta_3)u_0^2 + 2v^2 + 8u^2 + 18w^2$. Only the leading terms are shown. Neglected terms are small and of the first order (or smaller) in the submatrix involving only $\dot\beta_2, \dot\beta_3, \dot u_0, \dot v, \dot u, \dot w, q_1$, and q_2; of the third order (or smaller) in the submatrix involving only $\dot\varphi$, $\dot\chi, \dot\vartheta$, and q_3; and of the second order (or smaller) in the rest of the matrix.

	$\dot\beta_2$	$\dot\beta_3$	$\dot u_0$	$\dot v$	$\dot u$	$\dot w$	$\dot\varphi$	$\dot\chi$	$\dot\vartheta$	q_1	q_2	q_3
$\dot\beta_2$	1	0	0	0	0	0	0	0	0	0	0	0
$\dot\beta_3$	0	1	0	0	0	0	0	0	0	0	0	0
$\dot u_0$	0	0	$f^2(\beta_2, \beta_3)$	0	0	0	0	0	0	0	0	0
$\dot v$	0	0	0	2	0	0	0	0	0	0	0	0
$\dot u$	0	0	0	0	2	0	0	0	0	0	0	0
$\dot w$	0	0	0	0	0	2	0	0	0	0	0	0
$\dot\varphi$	0	0	0	0	0	0	$2v^2$	0	0	0	0	$2v^2$
$\dot\chi$	0	0	0	0	0	0	0	$2u^2$	0	0	0	$4u^2$
$\dot\vartheta$	0	0	0	0	0	0	0	0	$2w^2$	0	0	$6w^2$
q_1	0	0	0	0	0	0	0	0	0	$\mathcal{J}_1$	0	0
q_2	0	0	0	0	0	0	0	0	0	0	$\mathcal{J}_2$	0
q_3	0	0	0	0	0	0	$2v^2$	$4u^2$	$6w^2$	0	0	$\mathcal{J}_3$

B. The kinetic energy operator

The classical expression of the kinetic energy has the form

$$T = \frac{1}{2}\sum \mathcal{G}_{\mu\nu}\dot\xi_\mu\dot\xi_n u, \tag{3}$$

where $\dot\xi \equiv (\dot\beta_2, \dot\beta_3, \dot u_0, \dot v, \dot\chi, \dot u, \dot\varphi, \dot w, \dot\vartheta, q_1, q_2, q_3)$ and q_1, q_2, q_3 are the components of the angular velocity along the three axes of the intrinsic reference frame. As in I, we adopt here the convention of including the inertial coefficient B_λ in our amplitudes $a_\mu^{(\lambda)}$, which therefore would correspond to $\sqrt{B_\lambda}a_\mu^{(\lambda)}$ in the usual Bohr notation. The matrix elements of $\mathcal{G}$, approximated to the most relevant order, are shown in Table I. The determinant of this matrix turns out to be

$$\begin{aligned} G &\propto \left(\beta_2^2 + 2\beta_3^2\right)^2 f^4(\beta_2, \beta_3)u_0^2v^2u^2w^2 \\ &\equiv G_0(\beta_2, \beta_3)u_0^2v^2u^2w^2. \end{aligned} \tag{4}$$

The Pauli recipe for the quantization of the classical kinetic energy gives the Schrödinger equation

$$\sum_{\mu\nu}\frac{1}{g}\frac{\partial}{\partial\xi_\mu}\left[g\left(\mathcal{G}^{-1}\right)_{\mu\nu}\frac{\partial\Psi}{\partial\xi_\nu}\right] + \frac{2}{\hbar^2}\left[E - V(\xi)\right]\Psi = 0, \tag{5}$$

where $g^2 = G = \mathrm{Det}\,\mathcal{G}$ and ξ stays for the ensemble of the variables ξ_κ.

For our present purpose, we must specialize this general treatment [e.g., with a proper choice of the arbitrary function $f(\beta_2, \beta_3)$ in Eq. (2)], keeping in mind a necessary condition: The Schrödinger equation for the quadrupole amplitude, when the octupole amplitude is constrained to small values by a proper restoring potential, must converge to that of Bohr and therefore, at the critical point, to that of the X(5) model.[2] As

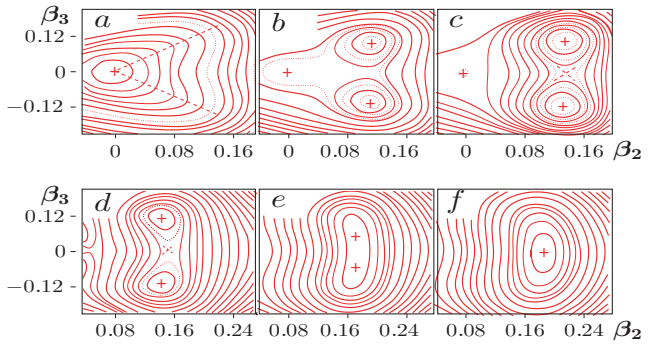

FIG. 2. (Color online) Potential-energy surfaces in the β_2-β_3 plane for several Th isotopes, as given by Nazarewicz *et al.* [24].

we shall see in Sec. IV A, this result is obtained with the choice

$$f(\beta_2, \beta_3) = \sqrt{\frac{\left(\beta_2^2 + \beta_3^2\right)\left(\beta_2^2 + 2\beta_3^2\right)}{\beta_2^2 + 5\beta_3^2}}, \tag{6}$$

from which one obtains

$$G_0(\beta_2, \beta_3) = \frac{\left(\beta_2^2 + \beta_3^2\right)^2\left(\beta_2^2 + 2\beta_3^2\right)^4}{\left(\beta_2^2 + 5\beta_3^2\right)^2}. \tag{7}$$

C. The critical potential in two dimensions

Possible landscapes of axial quadrupole-octupole deformation in the thorium region are exemplified in Fig. 2, where the potential energy is depicted as a function of the deformation parameters β_2 and β_3. Reported values have been obtained by Nazarewicz *et al.* [24] with a Wood-Saxon-Bogolyubov cranking calculation. We notice that Fig. 2(e) shows a potential minimum that is localized around a fixed value in the β_2 direction, whereas a flat minimum extends over a sizable interval in the β_3 direction. This is just the "critical" potential for the shape transition between octupole oscillation and permanent octupole deformation (combined with a fixed quadrupole deformation), corresponding to the Figs. 2(d) and 2(f), respectively. Figures 2(a), 2(b), and 2(c), instead, show a different kind of shape transition, proceeding directly from a fixed, reflection-asymmetric deformation [Fig. 2(c)] to quadrupole-octupole vibrations around a spherical shape [Fig. 2(a)].

The potential corresponding to the critical point is not shown. It should be somewhere between those depicted in Fig. 2(a) and Fig. 2(b). One can try to approximate the critical potential, as usual, with a square well, but now the flat bottom of the well should extend over a finite distance in β_2 and β_3, and be symmetric in β_3 around $\beta_3 = 0$. The shape of the borders is obviously relevant to the result. One could imagine shapes like those shown in Fig. 3 with dashed or dotted lines, but their description would involve at least two or three free parameters, and the comparison with experimental data could be not very significant. We have found, however, that good results are also

[2]This choice is different from the one adopted in I to describe the critical point in the octupole degree of freedom with a constant quadrupole deformation: In such a case, in fact, the proper limit for small octupole amplitudes does not correspond to the X(5) model but to the Frankfurt model [23], which is valid for small-amplitude octupole vibrations of a well-deformed nucleus.

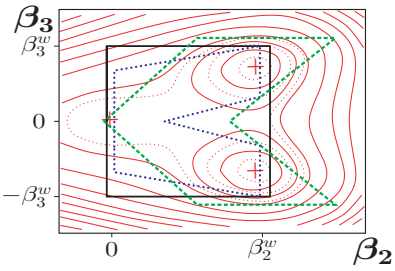

FIG. 3. (Color online) Possible shapes for a potential well simulating the critical-point potential. The potential-energy surface of Fig. 2(b) is also shown for comparison.

obtained with a simple rectangular shape (solid line in Fig. 3), implying only one free parameter, $b = \beta_3^w/\beta_2^w$ (apart from a common factor of scale).

IV. RESULTS AND COMPARISON WITH EXPERIMENTAL DATA

A. The energy eigenvalues

Now, as a first step, we can evaluate, as a function of b, the level energies in the ground-state band and deduce the best value of the parameter from a comparison with experimental results (Fig. 4). To proceed, we must make some assumptions on the behavior of axial and nonaxial modes of deformation. We will assume the following:

(i) Our choice of variables corresponds to independent degrees of freedom.
(ii) Nonaxial vibrations are confined to their lowest stationary state.
(iii) An approximation similar to that of the X(5) model is valid for the differential equations of all nonaxial amplitudes; that is, the differential equation in β_2, β_3 can be approximately decoupled from those concerning the other degrees of freedom.

Therefore, the complete wave function Ψ of Eq. (8) can be factored into three parts, as in Eq. (30) of I:

$$\Psi = \Psi_0(\beta_2, \beta_3)\Psi_1 Y_{JM}(\hat{\Omega}), \tag{8}$$

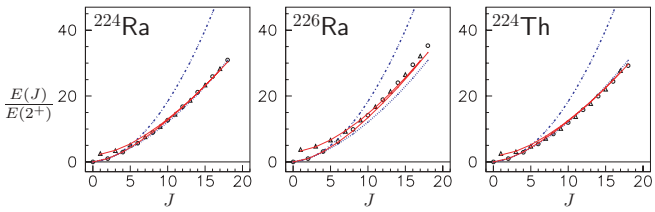

FIG. 4. (Color online) Experimental excitation energies of the positive-parity levels (circles) and of the negative-parity ones (triangles), in units of $E(2^+)$, for ^{224,226}Ra and ^{224}Th, compared with the results of the present model (full line) with the following values of the parameter $b = \beta_3^w/\beta_2^w$: 0.81 for ^{224}Ra, 0.68 for ^{226}Ra, and 0.85 for ^{224}Th. The predictions of the X(5) model (dotted lines) and for a rigid reflection-asymmetric rotor (dashed-dotted lines) are also shown for comparison.

where the function Ψ_1 depends on the deformation variables different from β_2, β_3.

From Eq. (4) we also know that the determinant G is factored in the same way. Then, the differential equation for β_2, β_3 takes the form

$$\left\{G_0^{-1/2}\left[\frac{\partial}{\partial\beta_2}\left(G_0^{1/2}\frac{\partial}{\partial\beta_2}\right)+\frac{\partial}{\partial\beta_3}\left(G_0^{1/2}\frac{\partial}{\partial\beta_3}\right)\right]+\epsilon - V(\beta_2,\beta_3) - \frac{J(J+1)}{3\left(\beta_2^2+2\beta_3^2\right)}\right\}\Psi(\beta_2,\beta_3) = 0. \tag{9}$$

This equation can be somewhat simplified with the substitution

$$\Psi_0(\beta_2,\beta_3) = g^{-1/2}\Phi(\beta_2,\beta_3), \tag{10}$$

where $g \propto G_0^{1/2}$, to obtain

$$\left\{\frac{\partial^2}{\partial\beta_2^2}+\frac{\partial^2}{\partial\beta_3^2}+\epsilon - V(\beta_2,\beta_3) - \frac{J(J+1)}{3\left(\beta_2^2+2\beta_3^2\right)} + V_g(\beta_2,\beta_3)\right\}\Phi(\beta_2,\beta_3) = 0, \tag{11}$$

with

$$V_g = \frac{1}{4g^2}\left[\left(\frac{\partial g}{\partial\beta_2}\right)^2+\left(\frac{\partial g}{\partial\beta_3}\right)^2\right] - \frac{1}{2g}\left[\frac{\partial^2 g}{\partial\beta_2^2}+\frac{\partial^2 g}{\partial\beta_3^2}\right]. \tag{12}$$

With the choice of $f(\beta_2,\beta_3)$ given in the Eq. (6), from Eq. (7) one obtains

$$g \propto \frac{\left(\beta_2^2+\beta_3^2\right)\left(\beta_2^2+2\beta_3^2\right)^2}{\left(\beta_2^2+5\beta_3^2\right)} \tag{13}$$

and, for $|\beta_3| \ll \beta_2$, $g \propto \beta_2^4[1+4(\beta_3/\beta_2)^4+\ldots]$. Therefore, the first and second derivative of g with respect to β_3 tend to zero when $|\beta_3| \ll \beta_2$ and, at the limit $\beta_3 \to 0$, $V_g = -2$ as in the original Bohr model. With the substitution $\Psi_0 = g^{-1/2}\Phi$, and the assumption that $V(\beta_2,\beta_3) = 0$ inside the potential well and $= +\infty$ outside, the differential equation to be solved takes the form

$$\left[\frac{\partial^2}{\partial\beta_2^2}+\frac{\partial^2}{\partial\beta_3^2}+\epsilon+V_g(\beta_2,\beta_3)\right]\Phi(\beta_2,\beta_3) = 0, \tag{14}$$

with V_g given in Eq. (12) and $\Phi = 0$ on the contour of the potential well. The numerical integration has been performed with the finite difference method. Namely, the space is discretized on a rectangular lattice and values of Φ at the lattice centers are taken as independent variables. In the place of second derivatives, the ratios of finite differences are used: For example,

$$\left(\frac{\partial^2\Phi}{\partial\beta_2^2}\right)_{x,y} \Rightarrow \frac{\Phi(x+\Delta_x,y)-2\Phi(x,y)+\Phi(x-\Delta_x,y)}{\Delta_x^2}.$$

As $\Phi(\beta_2,\beta_3) = (-1)^J\Phi(\beta_2,-\beta_3)$, it is enough to consider only the region $\beta_3 > 0$. The lattice centers are chosen as $\beta_2 = k_2\Delta_x$, $\beta_3 = (k_3-1/2)\Delta_y$ with $k_2 = 1,\ldots,n_2$, $k_3 = 1,\ldots,n_3$, and $\Delta_x = \beta_2^w/(n_2+1)$, $\Delta_y = 2\beta_3^w/(2n_3+1)$. The integration region is the upper rectangle with $0 < \beta_2 < \beta_2^w$, $0 < \beta_3 < \beta_3^w$. At the upper and lateral borders of the rectangle, the value of the eigenfunction must be zero.

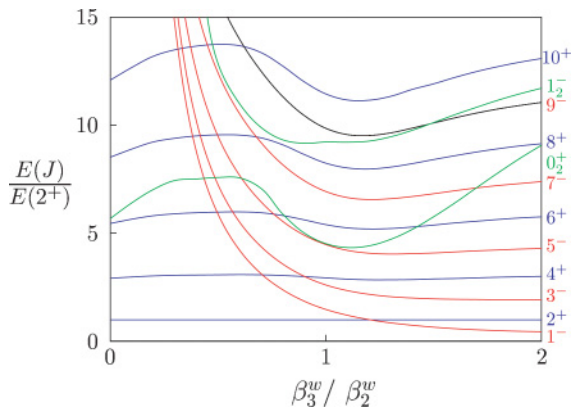

FIG. 5. (Color online) Calculated energies of excited levels of the ground-state and first excited bands, in units of $E(2_1^+)$, as a function of the ratio $b = \beta_3^w/\beta_2^w$.

The boundary conditions at $\beta_3 = 0$ are not specified, but to evaluate the approximate derivatives with respect to β_3 it is enough to consider the value of Φ at the line of centers immediately below zero, where they are either equal or opposite to the corresponding ones at $\beta_3 = \Delta_y/2$ according to the even or odd value of J.

The number of centers internal to the integration region—and therefore the number of independent values of Φ—is now $N = n_2 \cdot n_3$, and we obtain a finite dimensional $N \times N$ Hamiltonian matrix. This Hamiltonian has been diagonalized with the implicitly restarted Arnoldi-Lanczos method by using the ARPACK package [25].

In Fig. 5, calculated values of the excitation energies [in units of $E(2_1^+)$] are depicted as a function of the ratio $b = \beta_3^w/\beta_2^w$. At the limit for $\beta_3^w \to 0$, the curves corresponding to even J and π tend to the X(5) values, as expected. With increasing b, at the beginning these curves deviate substantially from the X(5) limit, but they come closer to the initial values for $b \approx 1$. In this region it is possible to find a good fit of the ground-state band of ^{224}Ra and of ^{224}Th, for $b = 0.81$ and for $b = 0.85$, respectively (Fig. 4).

Moreover, a rather good fit of the ground-state band of ^{226}Ra is obtained with $b = 0.68$ (i.e., close to the maximum of the curves for even parity and spin).

We can observe that, with our choice of the parameter b, the calculated 1^- level is always somewhat lower than the experimental one (Fig. 4). This fact can be related to the inclusion, in the potential well, of a region where β_3 remains large while β_2 tends to zero. Actually, the wave function of the first 1^- level extends appreciably in this region, at variance with other levels of the ground-state band.

It would be of great interest, of course, to extend the comparison to the lowest excited band with $K = 0$ [the $s = 2$ band in the X(5) model notation]. Unfortunately, in ^{224}Th no excited 0^+ level is known. The nonyrast level schemes of ^{224,226}Ra will be discussed in Sec. IV D.

B. Electromagnetic transition probabilities

Another important test for the model is provided by the $E2$ transition probabilities. The available experimental information on $B(E2)$ values is scarce (with only two transitions in ^{224}Ra and ^{226}Ra and one in ^{224}Th), but we hope our work can stimulate interest for new experimental investigations. The reduced matrix element of the quadrupole transition operator $\mathcal{M}(E2)$ between the states $|s, K = 0, J\rangle$ and $|s', K = 0, J'\rangle$ can be evaluated as

$$(sJ\|\mathcal{M}(E2)\|s'J') = C_2\langle sJ|\beta_2|s'J'\rangle(J\|Y_2\|J'), \quad (15)$$

with $\langle s, J|\beta_2|s', J'\rangle = \int \Psi_{sJ}\beta_2\Psi_{s',J'}\mathrm{d}\tau$ and C_2 constant. The volume element $\mathrm{d}\tau$, in our non-Cartesian coordinates, is the product of the differentials of the coordinate variables *multiplied by* $g = G^{1/2}$, with G the determinant of the matrix of inertia $\mathcal{G}$. In our assumptions, the integrals over all variables apart from β_2 ad β_3 are independent from one another and from the integral over $\mathrm{d}\beta_2\mathrm{d}\beta_3$, and their result is 1 (if the corresponding wave functions are properly normalized). As the electric dipole and quadrupole operators do not contain derivatives, we can exploit the substitution defined in Eq. (10) to express the remaining integral as

$$\int \Psi_{sJ}\beta_2\Psi_{s'J'}\mathrm{d}\tau = \int_0^{\beta_2^w}\mathrm{d}\beta_2\int_{-\beta_3^w}^{\beta_3^w}\mathrm{d}\beta_3\Phi_{sJ}\beta_2\Phi_{s'J'}. \quad (16)$$

This integral has been evaluated numerically, for values of $J \leqslant 18$, with $J' = J - 2$ (and also with $J' = J - 1$). The reduced matrix element over the angular coordinates has the form

$$(J\|Y_L\|J') = (-1)^J(4\pi)^{-1/2}\sqrt{(2J+1)(2L+1)(2J'+1)} \times \begin{pmatrix} J & L & J' \\ 0 & 0 & 0 \end{pmatrix}. \quad (17)$$

Finally, the reduced transition probabilities from J to J' are obtained as

$$B(E2, sJ \to s'J') = (2J+1)^{-1}(sJ\|\mathcal{M}(E2)\|s'J')^2.$$

The absolute values of the ratios of $E2$ reduced matrix elements, $R_J(E2) = (J\|\mathcal{M}(E2)\|J-2)/(2^+\|\mathcal{M}(E2)\|0^+)$, for transitions within the positive- and the negative-parity parts of the ground-state band, are depicted, as a function of $b = \beta_3^w/\beta_2^w$, in Fig. 6(a). Their limit at $\beta_3^w/\beta_2^w \to 0$ corresponds, as expected, to the X(5) value.

In addition to the in-band $E2$ transition, we have to consider the $E1$ transitions between levels of opposite parity. How to treat $E1$ transitions in the frame of the geometrical model is a big problem, as all $E1$ transition moments should vanish for a homogeneous fluid of constant charge density. In this sense, $E1$ transitions are outside the Bohr geometrical model. It is usual to assume a constant *electric polarizability* of the nuclear matter [27,28] to obtain the $E1$ operator in the form

$$\mathcal{M}(E1) = C_1\beta_2\beta_3Y_1. \quad (18)$$

This ansatz should be validated by proper microscopic calculations.

Actually, such a calculation has been performed by Tsvenkov *et al.* [29] for a number of radium, thorium, and uranium isotopes, in the frame of the Skyrme-Hartree-Foch model. The electric dipole moment turns out to be almost independent of the angular frequency in a given isotope, but it can change drastically (even in the sign) along the isotopic

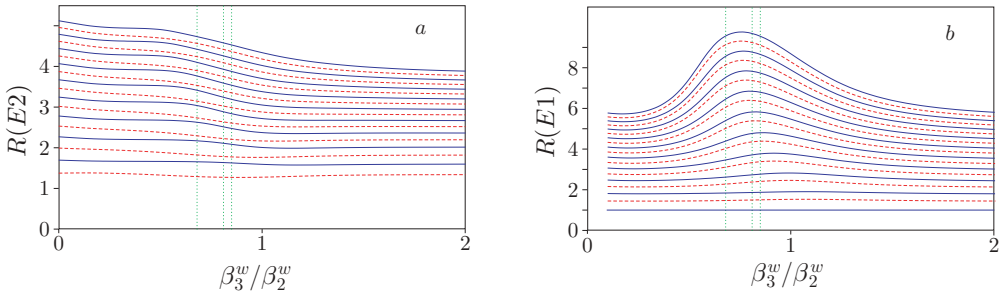

FIG. 6. (Color online) Absolute values of the ratios of reduced matrix elements of the electromagnetic transition operators, $R(EL, J_i) = \mathcal{M}(EL, J_i \to J_f)/\mathcal{M}(EL, L \to 0)$, with $J_f = J_i - L$, as a function of the parameter $b = \beta_3^w/\beta_2^w$. (a) $E2$ transitions; solid lines: even $J_i^+ \to J_f^+$, starting with $2^+ \to 0^+$ (from the bottom); dashed lines: odd $J_i^- \to J_f^-$, starting with $3^- \to 1^-$. (b) $E1$ transitions; solid lines: odd $J_i^- \to J_f^+$, starting with $1^- \to 0^+$ (from the bottom); dashed lines: even $J_i^+ \to J_f^-$, starting with $2^+ \to 1^-$. The vertical lines correspond to the adopted values of the parameter for ^{226}Ra, ^{224}Ra, and ^{224}Th ($b = 0.68$, 0.81, and 0.85, respectively).

chain. The small value of the electric dipole moments in ^{224}Ra is correctly predicted by these calculations.

Values of the ratios of the $E1$ matrix elements, $R_J(E1) = (J\|\mathcal{M}(E1)\|J-1)/(1^-\|\mathcal{M}(E1)\|0^+)$, obtained with the standard form [Eq. (18)] of the $E1$ operator, are shown in Fig. 6(b). They reach a maximum for β_3^w/β_2^w somewhat below 1, that is, just in a region including the values assumed for ^{224}Ra and ^{224}Th (0.81 and 0.85, respectively). The calculated values of $(J_i\|\mathcal{M}(EL)\|J_f)$ for $E2$ and $E1$ transitions in the ground-state bands of ^{224}Ra ($b = 0.81$), ^{226}Ra ($b = 0.68$), and ^{224}Th ($b = 0.85$) are given in the upper part of Table II. Values for the corresponding intraband transitions are very similar

TABLE II. Calculated values of the reduced matrix elements of $E1$ and $E2$ transitions in ^{224,226}Ra and ^{224}Th, normalized to those of the lowest lying transition of the same multipolarity.

$(J\|\mathcal{M}(E1)\|J')$				$(J\|\mathcal{M}(E2)\|J')$			
Transition	^{224}Ra	^{226}Ra	^{224}Th	Transition	^{224}Ra	^{226}Ra	^{224}Th
$1^- \leftrightarrow 0^+$	100	100	100	$2^+ \leftrightarrow 0^+$	100	100	100
$2^+ \leftrightarrow 1^-$	149	147	150	$3^- \leftrightarrow 1^-$	127	129	127
$3^- \leftrightarrow 2^+$	187	184	187	$4^+ \leftrightarrow 2^+$	164	166	163
$4^+ \leftrightarrow 3^-$	238	228	241	$5^- \leftrightarrow 3^-$	179	182	178
$5^- \leftrightarrow 4^+$	273	262	276	$6^+ \leftrightarrow 4^+$	211	217	209
$6^+ \leftrightarrow 5^-$	333	311	338	$7^- \leftrightarrow 5^-$	223	230	221
$7^- \leftrightarrow 6^+$	371	346	376	$8^+ \leftrightarrow 6^+$	252	264	248
$8^+ \leftrightarrow 7^-$	435	402	439	$9^- \leftrightarrow 7^-$	264	274	261
$9^- \leftrightarrow 8^+$	476	438	480	$10^+ \leftrightarrow 8^+$	289	304	284
$10^+ \leftrightarrow 9^-$	538	500	539	$11^- \leftrightarrow 9^-$	303	315	299
$11^- \leftrightarrow 10^+$	582	538	582	$12^+ \leftrightarrow 10^+$	325	342	320
$12^+ \leftrightarrow 11^-$	640	604	635	$13^- \leftrightarrow 11^-$	340	354	336
$13^- \leftrightarrow 12^+$	685	644	680	$14^+ \leftrightarrow 12^+$	360	377	354
$14^+ \leftrightarrow 13^-$	738	709	730	$15^- \leftrightarrow 13^-$	376	390	371
$15^- \leftrightarrow 14^+$	783	750	775	$16^+ \leftrightarrow 14^+$	393	411	388
$16^+ \leftrightarrow 15^-$	833	812	822	$17^- \leftrightarrow 15^-$	410	424	405
$17^- \leftrightarrow 16^+$	878	854	867	$18^+ \leftrightarrow 16^+$	426	443	421
$18^+ \leftrightarrow 17^-$	925	912	912	$19^- \leftrightarrow 17^-$	442	457	437
$0_2^+ \leftrightarrow 1_1^-$	84	42	150	$0_2^- \leftrightarrow 2_1^+$	8	24	6
$1_2^- \leftrightarrow 0_1^+$	31	31	31	$1_2^- \leftrightarrow 1_1^-$	38	37	38
$1_2^- \leftrightarrow 2_1^+$	49	50	47	$1_2^- \leftrightarrow 3_1^-$	42	43	43
$1_2^- \leftrightarrow 0_2^+$	22	63	21	$2_2^+ \leftrightarrow 0_1^+$	15	17	16
$2_2^+ \leftrightarrow 1_1^-$	113	86	111	$2_2^+ \leftrightarrow 2_1^+$	18	25	17
$2_2^+ \leftrightarrow 3_1^-$	143	103	142	$2_2^+ \leftrightarrow 4_1^+$	8	32	4
$2_2^+ \leftrightarrow 1_2^-$	33	71	34	$2_2^+ \leftrightarrow 0_2^+$	91	82	92

TABLE III. Experimental and calculated values of the ratios of reduced amplitudes of two $E1$ or two $E2$ transitions.

Transitions			$(J_A\|\mathcal{M}(EL)\|J'_A)/(J_B\|\mathcal{M}(EL)\|J'_B)$						
			^{224}Ra		^{226}Ra		^{224}Th		
	$J_A \to J'_A$	$J_B \to J'_B$	Exp.	Crit.	Exp.	Crit.	Exp.	Crit.	Rot.
$E1$	$1^-_1 \to 2^+_1$	$1^-_1 \to 0^+_1$	1.52 ± 0.14	1.50	1.36 ± 0.12	1.47	1.49 ± 0.26	1.50	1.42
$E1$	$3^-_1 \to 4^+_1$	$3^-_1 \to 2^+_1$			1.11 ± 0.18	1.24			1.15
$E2$	$4^+_1 \to 2^+_1$	$2^+_1 \to 0^+_1$	1.60 ± 0.05	1.63	≈ 1.76	1.66			1.60
$E2$	$1^-_2 \to 3^-_1$	$1^-_2 \to 1^-_1$	0.71 ± 0.10	1.10					–
$E1$	$1^-_2 \to 2^+_1$	$1^-_2 \to 0^+_1$	1.49 ± 0.16	1.57	1.24 ± 0.09	1.62			–
$E1$	$2^+_2 \to 3^-_1$	$2^+_2 \to 1^-_1$			1.29 ± 0.08	1.20			–

in the three cases, whereas the difference can be larger for the weak interband transitions, as shown in the lower part of the table.

C. Comparison with experimental transition probabilities

The Table III shows a few values of the ratio of reduced matrix elements for transitions of the same multipolarity that can be deduced from the available experimental information. In the same table, the corresponding values calculated with the present model are also shown (columns "Crit."), together with the ones expected for a reflection-asymmetric rigid rotor ("Rot.").

The most direct check of the model predictions would come from the ratios of $B(E2)$ values in the ground-state band. This is possible only in ^{224}Ra, and only for the decays of the lowest 2^+ and 4^+ levels. With the experimental values reported in the NNDC tabulation [26], $B(E2, 2^+ \to 0^+) = 97 \pm 3$ W.u. and $B(E2, 4^+ \to 2^+) = 138 \pm 8$ W.u., the experimental value of the ratio is 1.42 ± 0.09, which compares with the value 1.41 obtained from the calculated matrix elements of Tables II and III (for $b = 0.81$). Recall that, in the X(5) model [1], this ratio would be 1.59. For ^{226}Ra, the lifetime of the 4^+ state is known, but for the first excited state only an approximate value (without error estimate) is reported. Also in this case, the deduced ratio is consistent with the theoretical estimate (see Table III). These results are encouraging, but would obviously need to be validated by a more extensive check, involving higher lying levels, which, at the moment, is not possible.

A comparison of the two $E1$ transitions from the lowest level 1^- to the 0^+ and to the 2^+ states is possible for the three isotopes, as well as for the $E1$ branches from the 3^- in ^{226}Ra. All these amplitude ratios for transitions within the ground-state band, shown in the upper part of Table III, are in very good agreement with the calculated values. However, they are not significantly different from those expected for a rigid asymmetric rotor (as shown in the last column of Table III) nor from those reported by Lenis and Bonatsos [15] on the basis of a rather different model. We note that, when the transitions to be compared have the same multipolarity, the model predictions are parameter free, or—more exactly—only involve the model parameter β_3^w/β_2^w.

Instead, when the comparison concerns the ratios of the reduced matrix elements for $E1$ and $E2$ transitions de-exciting the same level, the model predictions include a further normalization factor [the ratio of constants C_1 and C_2 of

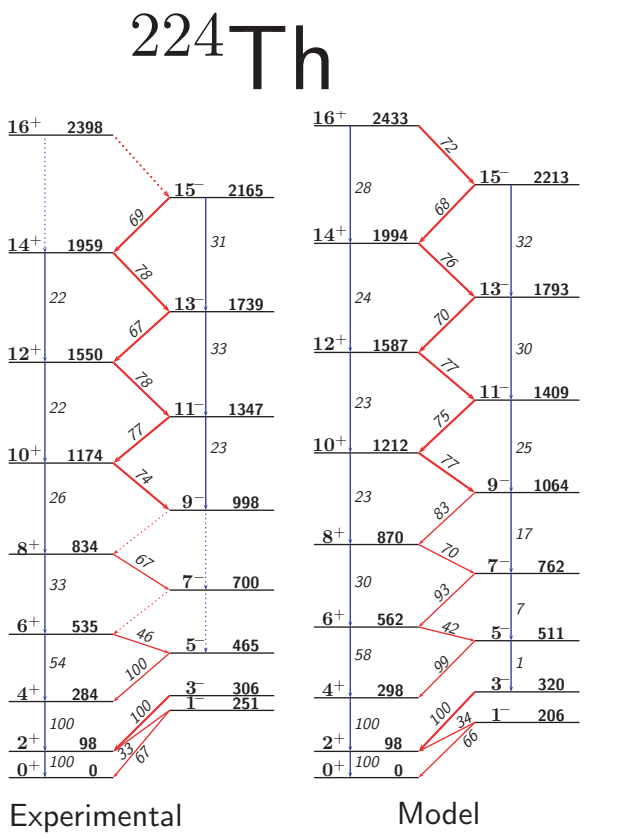

FIG. 7. (Color online) Level scheme of ^{224}Th, compared with the model predictions for $b = 0.85$. Calculated and experimental branching ratios are reported for each level. Experimental data are taken from the NNDC tabulation [26]. Experimental branching ratios from the 7^- and 9^- levels are not known. Theoretical values of the level energies (in keV) are normalized to that of the 2^+_1 level; those of the branching ratios are deduced from the matrix elements of Table II with the experimental values of the transition energies. Calculated branches lower than 1% are not shown.

TABLE IV. Experimental and calculated values of the ratios of reduced amplitudes of $E1$ and $E2$ transitions from the same level (in units of their Weisskopf estimates). The columns of calculated values are normalized to obtain the best fit to the experimental values for the transitions within the ground-state band.

Transitions		$[(\mathcal{M}(E1)/\mathcal{M}_W(E1))/(\mathcal{M}(E2)/\mathcal{M}_W(E2))] \times 10^3$								
		^{224}Ra			^{226}Ra			^{224}Th		
$E1$	$E2$	Exp.	Crit.	Rot.	Exp.	Crit.	Rot.	Exp.	Crit.	Rot.
$3^-_1 \to 2^+_1$	$3^-_1 \to 1^-_1$	0.69 ± 0.14	0.55	0.57						
$5^-_1 \to 4^+_1$	$5^-_1 \to 3^-_1$	0.98 ± 0.26[a]	0.63	0.60	1.36 ± 0.23[b]	2.13	2.42			
$6^+_1 \to 5^-_1$	$6^+_1 \to 4^+_1$							7.98 ± 1.17	7.18	8.21
$7^-_1 \to 6^+_1$	$7^-_1 \to 5^-_1$	0.56 ± 0.09	0.66	0.65	2.51 ± 0.15	2.23	2.56			
$8^+_1 \to 7^-_1$	$8^+_1 \to 6^+_1$	<1.22	0.68	0.66				7.19 ± 0.72	7.86	8.50
$9^-_1 \to 8^+_1$	$9^-_1 \to 7^-_1$	<1.71	0.71	0.67	2.82 ± 0.34	2.38	2.67			
$10^+_1 \to 9^-_1$	$10^+_1 \to 8^+_1$							7.78 ± 0.43	8.41	8.67
$11^-_1 \to 10^+_1$	$11^-_1 \to 9^-_1$				2.76 ± 0.27	2.53	2.67	9.35 ± 0.62	8.64	8.73
$12^+_1 \to 11^-_1$	$12^+_1 \to 10^+_1$				2.85 ± 0.25	2.62	2.68	9.06 ± 0.47	8.83	8.78
$13^-_1 \to 12^+_1$	$13^-_1 \to 11^-_1$				2.15 ± 0.29	2.70	2.70	8.45 ± 0.42	9.01	8.82
$14^+_1 \to 13^-_1$	$14^+_1 \to 12^+_1$				2.58 ± 0.17	2.79	2.71	9.84 ± 0.51	9.15	8.86
$15^-_1 \to 14^+_1$	$15^-_1 \to 13^-_1$				2.53 ± 0.17	2.94	2.73	9.69 ± 0.65	9.29	8.89
$17^-_1 \to 16^+_1$	$17^-_1 \to 15^-_1$				2.78 ± 0.43	2.98	2.74	10.47 ± 1.34	9.52	8.92
$18^+_1 \to 17^-_1$	$18^+_1 \to 18^+_1$				3.22 ± 0.21	3.05	2.74			
χ^2/n (with $n = 8$)						2.13	1.34		1.17	2.03
Confidence level (%)						<5	18		31	<5

[a]From NNDC [26] only. The $5^- \to 3^-$ (142-keV) γ ray observed in the reaction data [30] appears to be contaminated by a close-lying transition from a different reaction, as it results from the intensity mismatch in the $5^- \to 3^- \to 2^+(\to 1^-)$ cascade.
[b]From Ref. [31]. These data were not included in the fit.

Eqs. (15) and (18)], which needs to be determined from the experimental data. This comparison is therefore less direct, but it is perhaps more significant, as we shall see in the following.

Results concerning the $E1/E2$ branches in the ground-state band are shown in Table IV (and also depicted in Fig. 8). Experimental values of $E1/E2$ branching ratios in ^{224,226}Ra and ^{224}Th include those given in the NNDC tabulation [26,31] and later results from Ref. [30]. From these branching ratios we have deduced the absolute ratios—given in the "Exp." columns of Table IV—of the reduced matrix elements of $E1$ and $E2$ transitions, each of which is expressed in units of the corresponding Weisskopf estimate, $\mathcal{M}_W(EL) = (4\pi)^{-1/2}[3/(L+3)](1.2A^{1/3})^L e$ fm^L. In the same table are also shown the results of the model calculation at the critical point (Crit.), which have been normalized to obtain the best fit with the experimental values within the ground-state band of each nucleus. Values expected for a rigid asymmetric rotor (Rot.), normalized in the same way, are also shown. The ^{226}Ra point at $J_i = 5$, which, according to the authors themselves [31], could be considered as a lower limit, has not been included in the fits.

For the ground-state band of ^{224}Th (Figs. 7 and 8), we find a satisfactory agreement between the experimental values and the model predictions. In this case we have enough data to perform a χ^2 test of goodness of fit, and we obtain $\chi^2/N = 1.17$ with $N = 8$ degrees of freedom, corresponding to a confidence level of 31%. A fit with the rigid-rotor values would give a much larger value of $\chi^2/N = 2.03$ and a confidence level below 5%. Also for the ground-state band of

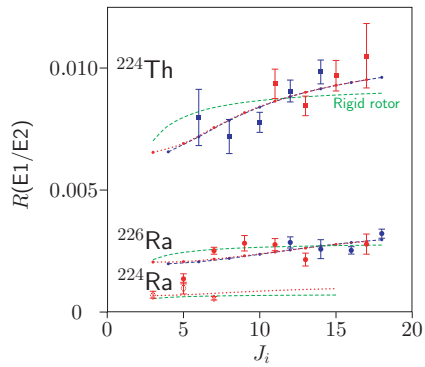

FIG. 8. (Color online) Ratios of the absolute value of the transition matrix elements (normalized to the Weisskopf unit) for $E1$ and $E2$ transitions in the ground-state bands of ^{224,226}Ra and ^{224}Th, from J_i to $J_i - 1$ and $J_i - 2$, respectively: $R_J(E1/E2) = (J_i \| [\mathcal{M}(E1) \| J_i - 1)/\mathcal{M}_W(E1)]/[(J_i \| \mathcal{M}(E2) \| J_i - 2)/\mathcal{M}_W(E2)]$. The dotted lines join the calculated values of the ratio (normalized to obtain the best fit with the ensemble of experimental values). The dashed lines join the values expected for a rigid rotor. The corresponding values deduced from the parameter-free model of Ref. [15] are (apart for a possible staggering between even and odd J_i) almost identical to the rotational ones for large values of J_i ($J_i > 7$) and, for decreasing values of J_i, their trend reaches a minimum around $J_i = 6$ and then increases slightly at lower values of J_i.

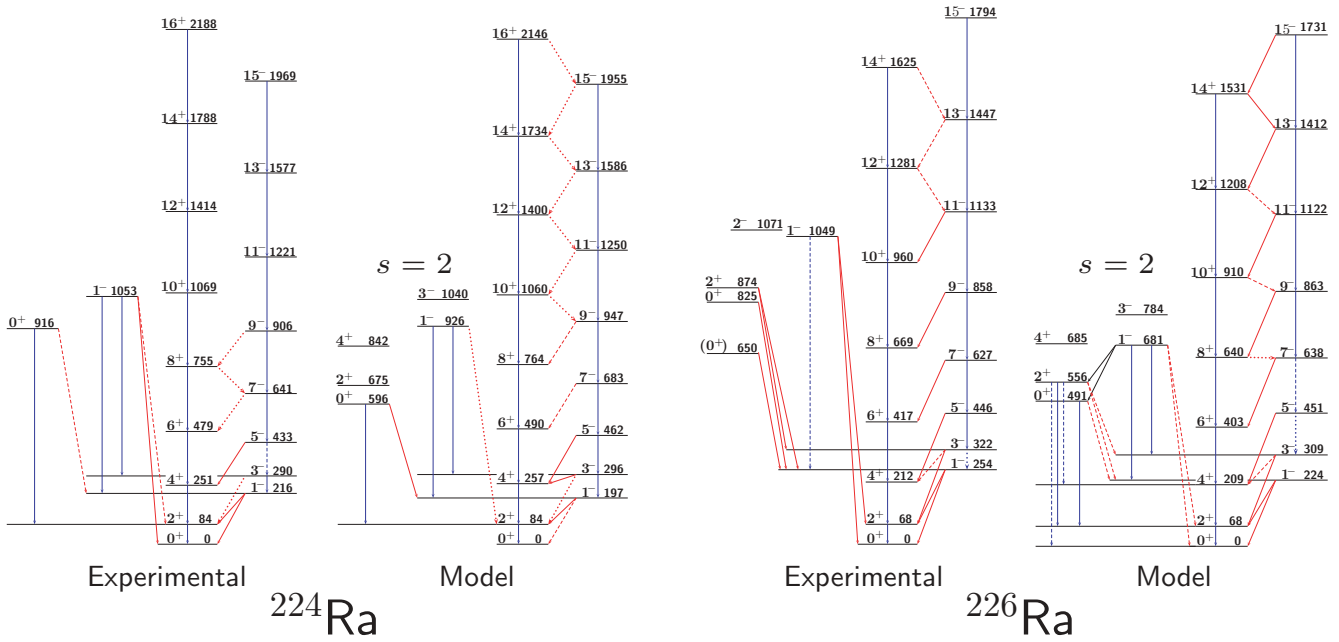

FIG. 9. (Color online) Partial level schemes of ^{224}Ra and ^{226}Ra, with the experimentally observed γ transitions, compared with the results of model calculations (with $b = 0.81$ and 0.68, respectively). Theoretical level energies (in keV) are normalized to that of the first excited level. Experimental energies for the lower levels of ^{224}Ra are taken from the NNDC tabulation [26]; those of the 10^+, 12^+, and higher levels are deduced from the γ-ray energies given by Cocks *et al.* [30]. For ^{226}Ra, those of levels up to 5^- are taken from NNDC or Ref. [31] and those of higher levels from Cocks *et al.* [30]. Gamma branches lower than 5% (or reported as upper limits) are shown as dotted lines, and those between 5% and 25% as dashed lines. Calculated branches lower than 1% are not shown. For a comparison of experimental $E1/E2$ branches with the model prediction at the critical point, see Table IV and Fig. 8.

^{224}Ra, the few available experimental values (or limits) are not far from the results of the model, but more experimental data would be necessary for a significant comparison. Actually, as was soon recognized [32–34], the $E1$ transitions in ^{224}Ra are rather weak compared to other nuclei in this region, and in particular their strengths are two orders of magnitude smaller than the corresponding ones in ^{224}Th.

Instead, experimental values for ^{226}Ra deviate significantly from the model predictions and approach those expected for a rigid rotor. This fact, combined with the slight upward deviation of level energies from the calculated curve for $J > 14$, suggests that the critical point of the phase transition in the Ra isotopic chain can be situated somewhere below $A = 226$, and probably close to $A = 224$.

D. The first excited $K = 0$ band

As anticipated in Sec. IV A, no experimental information is available for nonyrast levels of ^{224}Th. For ^{224,226}Ra isotopes, a few nonyrast levels are known from β^- decay of ^{224,226}Fr, from α decay of ^{228,232}Th, or from the ^{226}Ra(t, p) reaction. Unique assignments of the spin and parity have been reported only for some of them. Some of these levels, which could be considered as members of the excited $K = 0$ band [the $s = 2$ band in the X(5) expression], are reported, together with those of the yrast band, in Fig. 9, where also the main decay branches are indicated. In the same figure, the model-predicted levels, and their expected γ branches, are also shown.

We can immediately observe that nonyrast levels predicted by the model are always lower than the experimental ones (but a comparably large discrepancy is observed also in the $s = 2$ band of X(5) nuclei [2,3,7]). In the lower part of Table III, the calculated amplitude ratios for transitions from the excited $K = 0$ band are compared with the corresponding experimental ones, if the levels 0_2^+ and 1_2^- shown in Fig. 9 are interpreted as belonging to it. Only the ratio of the two $E1$ transitions from the 1_2^- level of ^{224}Ra and from the 2_2^+ level of ^{226}Ra are well consistent with the calculated value, whereas the corresponding ratios for the two $E1$ transitions from the 1_2^- level of ^{224}Ra and for the two $E2$ transitions from the 1_2^- level of ^{224}Ra seem to be significantly different from the model predictions (although the latter is subject to a large uncertainty, owing to the presence of a competing $M1$ component in the $1_2^- \to 1_1^-$ transition).

As for the $E1/E2$ ratios for interband transitions, it is not obvious that the value of the parameter C_1/C_2 ought to be the same as for transitions within the ground-state band, but if we assume it to be so, the $E1/E2$ ratios in the decay of the 1_2^- level of ^{226}Ra differ by a factor of 2 from the calculated values: The ratios to the $E2$ amplitude $1_2^- \to 3_1^-$, with the normalization used in Table IV, are $(0.75 \pm 0.7)10^{-3}$ for the $1_2^- \to 0_1^+$ $E1$ transition and $(1.05 \pm 0.07)10^{-3}$ for the $1_2^- \to 2_1^+$, which are to be compared with the theoretical values 0.29×10^{-3} and 0.46×10^{-3}, respectively.

Therefore, if the first two levels of the excited $s = 2$ band are tentatively identified with the 0_2^+ and 1_2^- levels of ^{224}Ra, their properties are not so well accounted for. One can hypothesize

different explanations for this fact. First, we remark that the identification of these levels as members of the β band can be put to a discussion. Actually, the 0_2^+ level could result from other (collective or noncollective) modes of excitation, such as, for example, pairing vibration [35,36], whereas the 1_2^- could correspond to (or be mixed with) the bandhead of the $K^\pi = 1^-$ band. Otherwise, the observed disagreement could indicate that our model is unable to correctly predict states outside the ground-state band, in particular if they are not far from levels of the nonaxial modes having the same J^π. The simultaneous investigation of axial and nonaxial modes, as has been performed via the extended coherent state model in Refs. [17–20], is outside our present possibilities.

V. CONCLUSIONS

An extension of Iachello's X(5) model to the axial quadrupole + octupole deformation has been developed with the formalism introduced in our previous paper I [10]. Assuming that both β_2 and β_3 can vary within a two-dimensional well with rectangular borders, and with a proper determination of a free function of the model, we have found the results to converge to those of X(5) when the interval available for β_3 tends to zero. The formalism is therefore suitable to describe the critical point of phase transitions involving axial quadrupole and octupole deformation at the same time.

As anticipated in I, the principal aim of this second part of our work was the description of the transitional nuclei ^{224}Ra and ^{224}Th, which were proposed to be close to such a critical point.

Actually, in spite of the admittedly crude schematization of the bidimensional potential, the relative values of the excitation energies of levels (of positive and negative parity) in the ground-state bands of both ^{224}Ra and ^{224}Th are satisfactorily reproduced by adjusting the only available parameter (the aspect ratio $b = \beta_3^w/\beta_2^w$ of the potential well). A good agreement is obtained with $b = 0.81$ for ^{224}Ra and with $b = 0.85$ for ^{224}Th. Moreover, a good agreement is also obtained for the first part of the ground-state band of ^{226}Ra with a lower value of the parameter, $b = 0.68$: Only above $J = 14$ do the experimental points deviate slightly from the calculated values, in the direction of the rigid-rotor curve (Fig. 4).

The (few) known ratios of transition strengths in the ground-state band for electromagnetic transitions of equal multipolarity (either $E2$ or $E1$) are in agreement with the model predictions. Unfortunately, only in a few cases can the ratio of the reduced strengths for transitions of equal multipolarity be deduced from the experimental data (see Table III) and in these cases the values expected at the critical point are not very different from those of the rotational model.

In some more cases, the relative strength of two transitions of different multipolarity ($E1$ and $E2$), coming from the same level, can be deduced from the measured branching ratio. The comparison with the model requires in this case one more parameter, which has been determined by a best-fit procedure (see Table IV and Fig. 8). But, in this case, the expected trend at the critical point is significantly different from that of a rigid rotator.

The calculated critical-point values of the ratios $E1/E2$ are in a rather good agreement with the experimental results in the case of ^{224}Th (Fig. 8), whereas for ^{226}Ra the trend of empirical values is closer to the one expected for a rigid rotor. For ^{224}Ra, the $E1$ transitions are very weak and experimental data are too scarce to permit a significant comparison with the model predictions.

New and more extensive measurements of the transition strengths either in ^{224}Ra or ^{224}Th would be highly desirable for a more significant test of the model.

[1] F. Iachello, Phys. Rev. Lett. **87**, 052502 (2001).
[2] R. F. Casten and N. V. Zamfir, Phys. Rev. Lett. **87**, 052503 (2001).
[3] R. Krucken *et al.*, Phys. Rev. Lett. **88**, 232501 (2002).
[4] P. G. Bizzeti and A. M. Bizzeti-Sona, Phys. Rev. C **66**, 031301(R) (2002).
[5] R. Clark *et al.*, Phys. Rev. C **68**, 037301 (2003).
[6] C. Hutter *et al.*, Phys. Rev. C **67**, 054315 (2003).
[7] D. Tonev, A. Dewald, T. Klug, P. Petkov, J. Jolie, A. Fitzler, O. Moller, S. Heinze, P. von Brentano, and R. F. Casten, Phys. Rev. C **69**, 034334 (2004).
[8] P. G. Bizzeti, in *Symmetries in Physics*, edited by A. Vitturi and R. Casten (World Scientific, Singapore, 2003), p. 262.
[9] P. G. Bizzeti and A. M. Bizzeti-Sona, in *Nuclear Theory 24*, edited by S. Dimitrova (Heron Press, Sofia, 2005), p. 311.
[10] P. G. Bizzeti and A. M. Bizzeti-Sona, Phys. Rev. C **70**, 064319 (2004).
[11] P. G. Bizzeti and A. M. Bizzeti-Sona, in *Symmetries and Low-Energy Phase Transition in Nuclear-Structure Physics*, edited by G. L. Bianco and D. Balabanski (University of Camerino, Italy, 2005), p. 87.
[12] P. G. Bizzeti and A. M. Bizzeti-Sona, in *Collective Motion and Phase Transitions in Nuclear Systems*, edited by A. A. Raduta, V. Baran, A. Gheorghe, and I. Ursu (World Scientific, Singapore, 2006), p. 3.
[13] P. G. Bizzeti and A. M. Bizzeti-Sona, in *Changing Facets on Nuclear Structure (Proceedings of the 9th International Spring Seminar on Nuclear Physics, Vico Equense 2007)*, edited by A. Covello (World Scientific, Singapore, 2007).
[14] D. Bonatsos, D. Lenis, N. Minkov, D. Petrellis, and P. Yotov, Phys. Rev. C **71**, 064309 (2005).
[15] D. Lenis and D. Bonatsos, Phys. Lett. **B633**, 474 (2006).
[16] N. Minkov, P. Yotov, S. Drenska, W. Scheid, D. Bonatsos, D. Lenis, and D. Petrellis, Phys. Rev. C **73**, 044315 (2006).
[17] A. A. Raduta, L. Pacearescu, and V. Baran, Phys. Rev. C **67**, 014301 (2003).
[18] A. A. Raduta and C. Raduta, Nucl. Phys. **A768**, 170 (2006).
[19] A. A. Raduta, A. H. Raduta, and C. M. Raduta, Phys. Rev. C **74**, 044312 (2006).
[20] A. Raduta and C. Raduta, in *Collective Motion and Phase Transitions in Nuclear Systems*, edited by A. Raduta, V. Baran,

A. Gheorghe, and I. Ursu (World Scientific, Singapore, 2006), p. 21.
[21] D. A. Bohr, Dan. Mat. Phys. Medd. **26**, n. 14 (1952).
[22] C. Wexler and G. G. Dussel, Phys. Rev. C **60**, 014305 (1999).
[23] J. Eisenberg and W. Greiner, *Nuclear Theory*, Vol. I, 3rd ed. (North-Holland, Amsterdam, 1987).
[24] W. Nazarewicz and P. Olanders, Nucl. Phys. **A441**, 420 (1985).
[25] http://www.caam.rice.edu/software/arpack/.
[26] http://www.nndc.bnl.gov/.
[27] D. A. Bohr and B. Mottelson, Nucl. Phys. **4**, 529 (1957).
[28] D. A. Bohr and B. Mottelson, Nucl. Phys. **9**, 687 (1958).
[29] A. Tsvenkov, J. Kvasil, and R. Nazmitdinov, J. Phys. G **28**, 2187 (2002).
[30] J. Cocks *et al*., Nucl. Phys. **A645**, 61 (1999).
[31] B. Ackermann *et al*., Nucl. Phys. **A559**, 61 (1993).
[32] M. Marten-Toelle, B. Ackermann, H. Baltzer, T. Bihn, V. Grafen, C. Guenther, H. Hausmann, N. Singh, R. Toelle, J. de Boer *et al*., Z. Phys. A **336**, 27 (1990).
[33] P. Butler and W. Nazarewicz, Nucl. Phys. **A533**, 249 (1991).
[34] E. Egido and L. Robledo, Nucl. Phys. **A524**, 65 (1991).
[35] C. Friedman, K. Katori, D. Albright, and J. Schiffer, Phys. Rev. C **9**, 760 (1974).
[36] W. van Rij and S. H. Kahana, Phys. Rev. Lett. **28**, 50 (1972).